Journal of the European Ceramic Society 41 (2021) 424–429

Contents lists available at ScienceDirect

Journal of the European Ceramic Society

journal homepage: www.elsevier.com/locate/jeurceramsoc

Cold sintered, temperature-stable $CaSnSiO_5$-K_2MoO_4 composite microwave ceramics and its prototype microstrip patch antenna

Yuping Ji [a], Kaixin Song [a,b,*], Shiyu Zhang [c], Zhilun Lu [b,d], Ge Wang [b], Linhao Li [b], Di Zhou [e], Dawei Wang [b,*], Ian M. Reaney [b,*]

[a] College of Electronics Information, Hangzhou Dianzi University, Hangzhou, 310018, China
[b] Department of Materials Science and Engineering, University of Sheffield, Sheffield, S1 3JD, UK
[c] Wolfson School of Mechanical, Electrical and Manufacturing Engineering, Loughborough University, Loughborough, LE11 3TU, UK
[d] The Henry Royce Institute, Sir Robert Hadfield Building, Sheffield, S1 3JD, UK
[e] Electronic Materials Research Laboratory, Key Laboratory of the Ministry of Education & International Center for Dielectric Research, School of Electronic Science and Engineering, Xi'an Jiaotong University, Xi'an, 710049, Shaanxi, China

ARTICLE INFO

Keywords:
Microwave dielectric
Cold sintering process
Microstrip patch antenna

ABSTRACT

Dense (1-x)wt%$CaSnSiO_5$-xwt%K_2MoO_4 (CSSO-KMO) composite ceramics were fabricated by the cold sintering process at 180 °C under 400 MPa for 60 min. X-ray diffraction, Energy dispersive X-ray and Raman spectroscopy confirmed that CSSO and KMO coexisted without intermediate phases. As KMO weight fraction increased, relative permittivity (ε_r) and temperature coefficient of resonant frequency (τ_f) decreased and the microwave quality factor ($Q\times f$, where f is resonant frequency) increased. Near-zero τ_f (-0.5 ppm/°C) was obtained for 65 wt %CSSO-35 wt%KMO with $\varepsilon_r \sim 9.2$ and $Q\times f \sim 6240$ GHz. No chemical reaction between ceramic composites and silver was observed, demonstrating potential for cofiring with Ag-paste. A prototype antenna was fabricated from 65 wt%CSSO-35 wt%KMO composite ceramic with a bandwidth of 144 MHz @ -10 dB, a gain of 5.7 dBi and a total efficiency of 88.4 % at 5.2 GHz, suitable for 5 G mobile communication systems.

1. Introduction

Microwave dielectric ceramics are commonly used in communication systems in components such as antennas, duplexers, resonators and substrates [1,2]. With the development of fifth-generation technology for cellular networks (5 G), faster and more reliable broadband access is required with larger capacity and shorter transmission response time (delay less than 1 ms). To reduce the signal delay of the system, it is necessary to optimize the signal transmission response mode, system structure and physical hardware. The propagation speed of electromagnetic waves is inversely proportional to the relative permittivity (ε_r) and low ε_r values minimize the cross-coupling between air and dielectrics for 5 G applications. At the same time, high microwave quality factor ($Q\times f$, where f is the resonant frequency) improves selectivity and energy transmission, and near zero temperature coefficient of resonant frequency (τ_f) maintains temperature stability of components in operation [3–10]. Temperature-stable silicates such as $Ca_2Al_2SiO_7$ [11], $Y_3MgAl_3SiO_{12}$ [12], Mg_2SiO_4 [13] and (Sr,Ba)$Y_2Si_3O_{10}$ [14] with low ε_r (4~15) and high $Q\times f$ (20,000~240,000 GHz) have therefore, attracted attention as candidates for 5G applications. However, silicate-based ceramics are conventionally sintered at high temperatures (> 1200 °C), consuming energy and releasing carbon. The cold sintering process (CSP) can densify ceramics and composites at ultralow temperatures (< 200 °C), temperatures that not only reduce carbon emissions but also facilitate direct deposition onto printed circuit boards [15–27].

$CaSnSiO_5$ (CSSO) is conventionally sintered at 1450 °C with $\varepsilon_r \sim 10.9$, $\tau_f \sim 35$ ppm/°C, $Q\times f \sim 43{,}600$ GHz [28,29] and is therefore, an ideal base to begin the search for cold sintered silicates. However, initial cold sintering studies of CSSO were unsuccessful and hence, following work by Wang and co-workers [26,27], K_2MoO_4 (KMO) was used as a fluxing agent to encourage densification and to tune τ_f to near zero. The microstructure, Ag compatibility and microwave dielectric properties of CSSO-KMO composites were therefore, investigated followed by the design, fabrication and testing of a prototype microstrip patch antenna on substrates made from optimum compositions.

* Corresponding authors at: College of Electronic Information, Hangzhou Dianzi University, Hangzhou, 310018, China. Department of Materials Science and Engineering, University of Sheffield, Sheffield, S1 3JD, UK.
E-mail addresses: kxsong@hdu.edu.cn (K. Song), daiwei.wang@sheffield.ac.uk (D. Wang), i.m.reaney@sheffield.ac.uk (I.M. Reaney).

https://doi.org/10.1016/j.jeurceramsoc.2020.08.053
Received 15 June 2020; Received in revised form 17 August 2020; Accepted 22 August 2020
Available online 25 August 2020

2. Experimental Section

(1-x)wt%CSSO-xwt%KMO (x = 20, 30, 35, 40, 50, 60, 70, 80, 90 and 100) composite ceramics were prepared by CSP. CSSO powder was synthesized by a traditional high-temperature solid-state method. The raw materials, $CaCO_3$ (Acros Organics, 99.99 %), SiO_2 (Acros Organics, 99.99 %) and SnO_2 (Acros Organics, 99.99 %) were weighed according to the stoichiometric ratio of $CaCO_3$: SiO_2: SnO_2 = 1:1:1, and then planetary ball-milled 4 h in isopropanol. The mixed powders were dried and calcined at 1450 °C for 4 h to synthesize the CSSO powders. To obtain fine and uniform CSSO powders, the calcined CSSO powders were re-milled 4 h, dried, and then sieved using a 48 μm Nylon screen. CSSO and KMO (Alfa Aesar, > 99 %) powders were weighed and mixed with ~15 wt% deionized water. CSSO-KMO composite ceramics were obtained by hot-pressing mixed powders in a 12 mm die at 180 °C for 60 min under a uniaxial pressure of 400 MPa, after which samples were placed in an oven at 120 °C for 24 h to remove residual moisture. Furthermore, in order to reveal the chemical compatibility, a Heraeus LTC3602 low temperature Ag paste was printed between two green pellets, and then cofired by cold sintering to form a sandwich structure.

The geometric method was used to calculate the bulk density of composite ceramics [30–32]. X-ray powder diffraction (XRD, D2 Phaser, Bruker) using CuK_α radiation was employed to identify crystal structure and phase composition. Scanning electron microscope (SEM, Inspect F50, FEI) equipped with energy dispersive spectroscopy (EDS) was used to examine the microstructure on the polished surface and cross section of composite ceramics. Raman spectra were collected at room temperature using a Raman spectrometer (LabRAM HR800) excited with an Ar^+ laser (514.5 nm). Temperature and frequency dependence of ε_r was measured using an Agilent 4294A impedance analyzer from room temperature to 250 °C. Impedance spectroscopy was performed using an Agilent E4980A impedance AC analyzer from 20 to 10^6 Hz. A vector network analyzer (R3767CH, Advantest Corporation, Tokyo, Japan) was measured the microwave properties of the composite ceramics by the $TE_{01}\delta$ dielectric resonator method. The cavity was heated by Peltier device and the resonance frequency (f) was measured in the range from 25 to 85 °C. The following formula was used to obtain the corresponding τ_f value:

$$\tau_f = \frac{f_T - f_{T0}}{f_{T0} \times (T_T - T_{T0})} \times 10^6 (ppm/℃) \quad (1)$$

where f_{T0} and f_T represent f at T_0 (25 °C) and T (85 °C), respectively.

3. Results and discussion

Fig. 1 shows the XRD patterns of synthesized CSSO powder, KMO raw powder and cold-sintered CSSO-KMO composites. Both CSSO (space group *A2/a,* JCPDS No.86−0928) and KMO (space group *C12/m1,* JCPDS No.29–1021) have a monoclinic structure [26–29]. All diffraction peaks in the XRD patterns belong to CSSO and KMO with no peaks from impurity phases detected. The intensity of KMO peaks increases as a function of its weight fraction.

Fig. 2 displays the Raman spectra of cold-sintered (1-x)CSSO-xKMO composite ceramics at room temperature. According to group theory and irreducible representation, CSSO and KMO have 45 and 39 different vibration modes, respectively.

$$\Gamma_{CSSO} = 9A_g + 11A_u + 12B_g + 13B_u \quad (2)$$

$$\Gamma_{KMO} = 13A_g + 7A_u + 8B_g + 11B_u \quad (3)$$

The main Raman bands of CSSO are located at 135, 175, 295, 323, 363, 443, 510, 572 and 740 cm^{-1}, which are attributed to bending modes of the Ca-O bond (135, 175 and 295 cm^{-1}), $[SiO_4]^{4-}$ modes (443 and 510 cm^{-1}) and $[SnO_6]$- polyhedral modes (323, 363, 572 and 740 cm^{-1}) [33,34]. For KMO, Raman bands of 100 ~ 160 cm^{-1} are attributed to translations and vibrations modes of MoO_4 tetrahedra and translations of K^+, bands at 310 ~ 370 cm^{-1} belong to bending modes of MoO_4 tetrahedra and modes at 820 ~ 890 cm^{-1} are assigned to stretching modes of MoO_4 tetrahedra [35,36]. As KMO concentration increases, the intensity of KMO Raman modes increases (as marked in orange frame) and all data except the end-members remains consistent with a two-phase mix with CSSO.

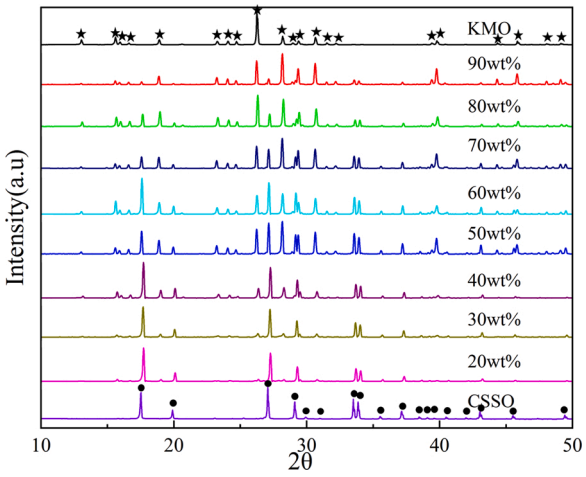

Fig. 1. Room-temperature XRD patterns of (1-x)CSSO-xKMO composite ceramics fabricated by CSP, and CSSO powder synthesized by solid state reaction.

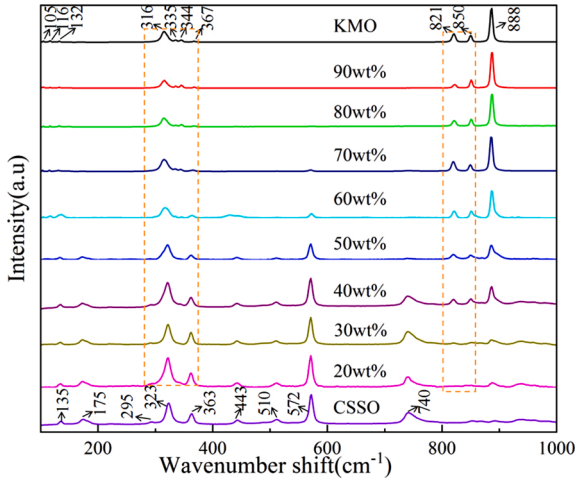

Fig. 2. Raman spectra of (1-x)CSSO-xKMO composite ceramics.

Fig. 3(a) presents the SEM images of cold-sintered 70 wt%CSSO-30 wt%KMO composite ceramics. EDS spectra showed the elongated needle or sheet-shaped radial grains belong to KMO (indexed triangle shape), and the aggregated grains are CSSO (indexed circle shape). To verify the compatibility of cold-sintered (1-x)CSSO-xKMO composite ceramics with Ag electrodes, Ag powder was cold-sintered with 65 wt% CSSO-35 wt%KMO powder, Fig.3(b). The white area is the Ag electrode layer, which has a clean interface with CSSO-KMO ceramic particles. EDS line scans suggest that there is no interact between Ag and CSSO-KMO composite, Fig. 4(c), indicating good chemical compatibility with Ag electrode.

The relative density (ρ_r) and microwave dielectric properties of (1-x) CSSO-xKMO composite ceramics as a function of KMO weight fraction are plotted in Fig. 4. ρ_r increases from 89 % for 80 wt%CSSO-20 wt% KMO to near 100 % for KMO. ε_r and τ_f decrease linearly as KMO weight fraction increases, while Q×f increases, Table 1. Near-zero τ_f (-0.5 ppm/°C) is obtained for 65 wt%CSSO-35 wt%KMO composites with ε_r ~

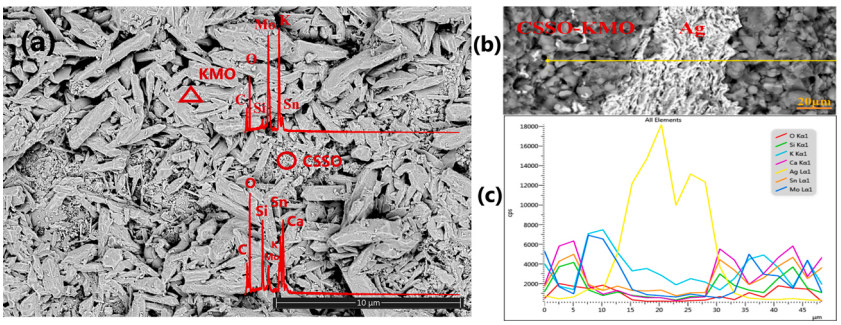

Fig. 3. (a) SEM and EDS of etched polished surface of 70 wt%CSSO-30 wt%KMO sample (Triangle KMO, Circle CSSO); (b) SEM of the cross section of 65 wt%CSSO-35 wt%KMO sample co-sintered with silver, and (c) EDS elemental line.

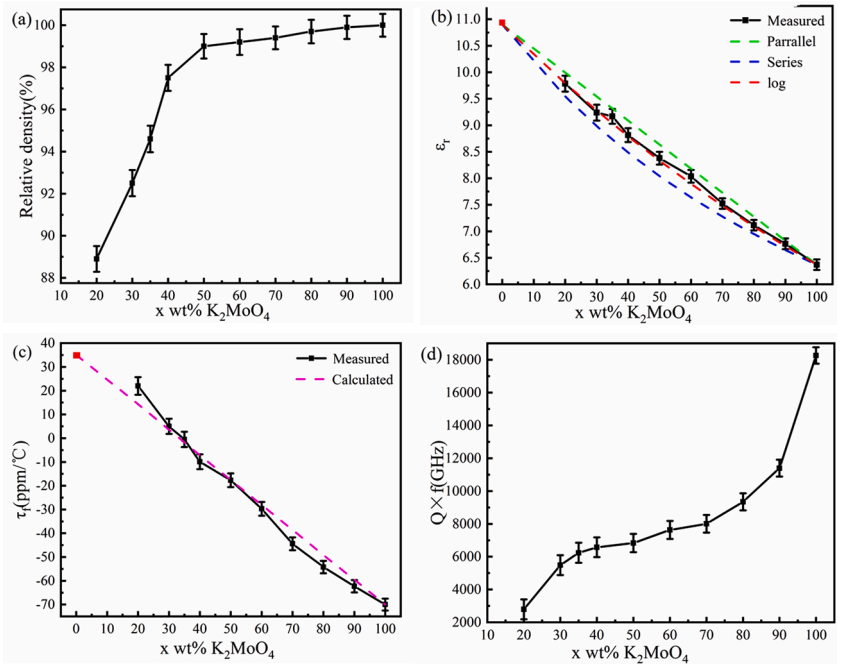

Fig. 4. Microwave dielectric properties of (1-x)CSSO-xKMO composite ceramics as a wt fraction of KMO.

9.168 and $Q{\times}f \sim 6240$ GHz. According to the XRD, Raman and EDS, there are no chemical interactions between the two phases. Thus, the effective ε_r can be estimated by the Lichtenecker mixing law [37]:

$$\text{parallel mixing law, } \varepsilon = V_1\,\varepsilon_1 + V_2\,\varepsilon_2 \tag{4}$$

$$\text{series mixing law, } 1/\varepsilon = V_1\,/\varepsilon_1 + V_2\,/\varepsilon_2 \tag{5}$$

$$\text{logarithmic mixing law, } \varepsilon = \varepsilon 1 v 1 \varepsilon 2 v 2 i.e., \lg\varepsilon = V 1 \lg\varepsilon 1 + V 2 \lg\varepsilon 2 \tag{6}$$

Table 1
Sintering temperature (ST), relative density (ρ_r), and microwave dielectric properties of (1-x)CSSO-xKMO ceramics.

Composition	ST(℃)	ρ_r(%)	ε_r	$Q{\times}f$ (GHz)	τ_f (ppm/℃)
$CaSnSiO_5$	1450	95	10.9	43,600	+35
20 wt%K_2MoO_4	180	89	9.78	2792	+22
30 wt%K_2MoO_4	180	93	9.24	5484	+5
35 wt%K_2MoO_4	180	95	9.17	6240	−0.5
40wt%K_2MoO_4	180	98	8.82	6576	−9.9
50wt%K_2MoO_4	180	99	8.38	6831	−18
60wt%K_2MoO_4	180	99	8.04	7628	−30
70 wt%K_2MoO_4	180	99	7.52	8004	−44
80 wt%K_2MoO_4	180	100	7.12	9343	−54
90wt%K_2MoO_4	180	100	6.76	11,395	−62
K_2MoO_4	150	100	6.37	18,266	−70

where ε_1 and ε_2 are the dielectric constants of phase 1 and phase 2, respectively. V_1 and V_2 ($V_1 + V_2 = 1$) are the volume fractions of phase 1 and phase 2 respectively. From Fig. 4(b), ε_r of (1-x)CSSO-xKMO composite ceramics is less than the calculated value of Eq. (4), larger than the calculated value of Eq. (5), and close to that obtained using Eq. (6), which shows that ε_r follows the logarithmic mixing law. τ_f may be predicted according to parallel mixing rules,

$$\tau_f = V_1\tau_{f1} + V_2\tau_{f2} \tag{7}$$

where τ_{f1} and τ_{f2} correspond to the τ_f of phase 1 and phase 2, respectively, as presented in Fig. 4(c).

Fig. 5 shows the temperature dependence of ε_r for 65 wt%CSSO-35 wt%KMO measured from 10 kHz to 1 MHz. ε_r is stable from room temperature to 250 °C, as shown in Fig. 7a, indicating no phase transition in this temperature range but decreases with increase in frequency as space charge contributions diminish (Fig. 5b). At room temperature, ε_r @ 1 MHz is 10.8, close to the value at microwave frequencies in Table 1 (9.17).

Room temperature EIS of 65 wt%CSSO- 35 wt%KMO is shown in Fig. 6. The complex impedance is divided into real part (Z') and imaginary part (Z'') and is expressed by the following formula.

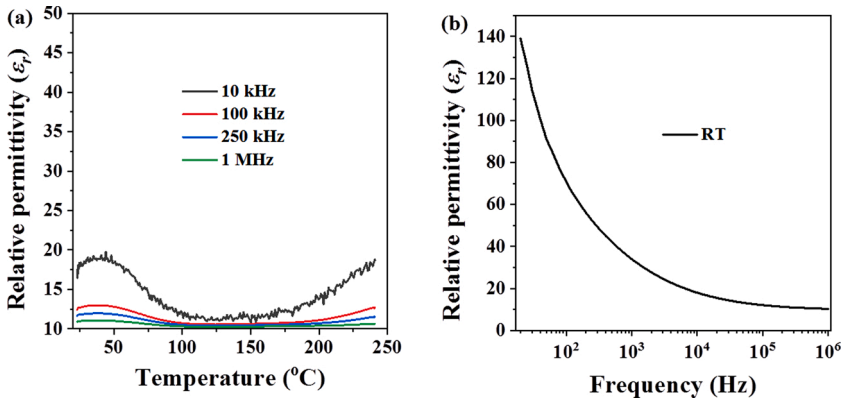

Fig. 5. (a) Temperature dependence, (b) Frequency dependence of ε_r for 65 wt%CSSO- 35 wt%KMO ceramic.

$$Z = \frac{R}{1 + i\omega RC} = Z' - iZ'' \quad (8)$$

$$Z' = \frac{R}{1 + (\omega RC)2} \quad (9)$$

$$Z'' = \frac{\omega R2C}{1 + (\omega RC)2} \quad (10)$$

where ω is angular frequency. From Fig. 7(a), the observed non-perfect semicircle is equal to the sum of two smaller semicircles, corresponding to two Debye peaks in frequency dependence of Z" and M", Fig. 6(b), which indicates at least two electrical components. The extracted capacitances of these two components are 2.6×10^{-12} F cm^{-1} and 1.7×10^{-12} F cm^{-1} for component 1 and 2, respectively. The complex microstructure of the CSSO – KMO make attributing the components to a specific part of the microstructure difficult but the low temperature, low frequency response is consistent with the space-charge contribution observed in the LCR data, Fig. 5, which decreases with increasing frequency and is absent in MW measurements, Fig. 4.

A 5 G prototype microstrip patch antenna (MSPA) with a center operating frequency of 5.2 GHz was designed and fabricated using the 65 wt%CSSO-35 wt%KMO ceramic as a substrate. The radiation element (the patch) and the ground plane was made of adhesive copper tape. The patch had the dimensions of 11.71 mm x 11.55 mm and the feed point was 3.75 mm away from the patch edge. A semi-rigid coaxial cable (RG405) was used for providing the probe feeding. The thickness of 65 wt%CSSO-35 wt%KMO ceramic substrate was 1.45 mm. The fabricated MSPA is shown in the inset pattern of Fig. 7(a).

The measured and simulated S11 result is shown in Fig. 7(a), indicating a good agreement between the measurement and simulation. The MSPA also shows the good impedance match, with a -10 dB bandwidth of 144 MHz. The MSPA was measured in a Spherical Near-Field anechoic chamber. The measured radiation patterns at 5.2 GHz at two principle cut planes: magnetic plane (H-plane) and electric plane (E-plane) are shown in Fig. 7(b) and Fig. 7(d), respectively, compared with simulated results. Good agreement between simulation and measurement is observed. The measured antenna gain, directivity and total efficiency (including the impedance mismatch) are shown in Fig. 7(c). The MSPA has an antenna gain of 5.7 dBi and total efficiency of 88.4 % at 5.2 GHz. The far-field performance suggests that 65 wt%CSSO-35 wt%KMO is a good candidate for antenna applications.

4. Conclusions

(1-x)CSSO-xKMO microwave composite ceramics with 89 %–100 % relative density were successfully fabricated by CSP (180 °C, 60 min and 400 MPa). SEM showed that the composite ceramics had a dense microstructure. XRD, EDS and Raman spectra identified two discrete phases of CSSO and KMO, with no chemical interaction. With increasing weight fraction of KMO, ε_r and τ_f decreased, while $Q \times f$ increased. A near-zero $\tau_f \sim$ -0.5 ppm/°C was obtained in 65 wt%CSSO-35 wt%KMO with $\varepsilon_r \sim$ 9.17 and $Q \times f \sim$ 6240 GHz. ε_r was stable from room temperature to 250 °C but decreased in respect to frequency, consistent with a low temperature, low frequency space charge contribution observed in EIS data. CSSO-KMO composite ceramics and Ag electrodes had good compatibility. A MSPA was designed and fabricated using cold sintered 65 wt%CSSO-35 wt%KMO as a substrate with a central operating frequency of 5.2 GHz. The antenna had an S11 of -10 dB with bandwidth of 144 MHz. The antenna gain of the MSPA was 5.7 dBi at 5.2 GHz, and the total efficiency was 88.4 %.

Declaration of Competing Interest

The authors declare that they have no known competing financial

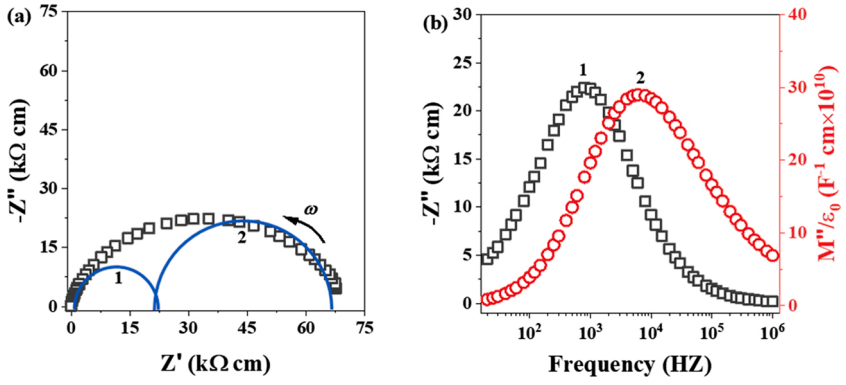

Fig. 6. (a) Z* plot, and (b) Frequency dependence of Z" and M" for 65 wt%CSSO- 35 wt%KMO ceramic.

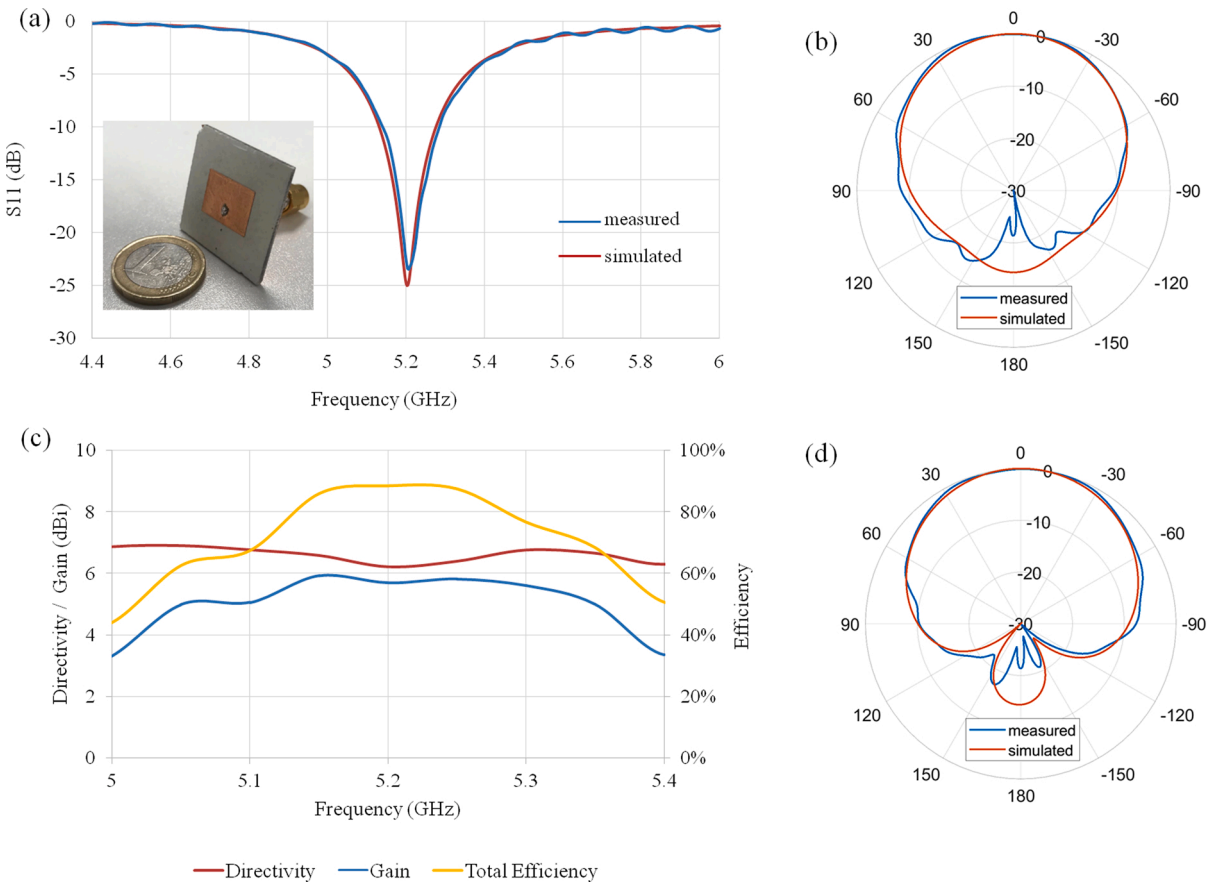

Fig. 7. (a) Measured S11 result of MSPA, compared with the simulation; (c) Measured far-field performance of the MSPA; Radiation patterns of the MSPA at (b) H-plane, (d) E-plane.

interests or personal relationships that could have appeared to influence the work reported in this paper.

Acknowledgement

This work was supported by the National Natural Science Foundation of China (51672063), the training plan for young and middle-aged key teachers of Hangzhou Dianzi University, the Engineering and Physical Sciences Research Council of UK (EP/N010493/1 and EP/L017563/1) and the Henry Royce Institute for Advanced Materials (funded through EPSRC grants EP/R00661X/1, EP/S019367/1, EP/P02470X/1 and EP/P025285/1).

References

[1] R.J. Cava, Dielectric materials for applications in microwave communications, J. Mater. Chem. 11 (11) (2001) 54–62.
[2] I.M. Reaney, D. Iddles, Microwave dielectric ceramics for resonators and filters in mobile phone networks, J. Am. Ceram. Soc. 89 (7) (2006) 2063–2072.
[3] J.B. Song, K.X. Song, J.S. Wei, H.X. Lin, J. Wu, et al., Ionic occupation, structures, and microwave dielectric properties of Y3MgAl3SiO12 garnet-type ceramics, J. Am. Ceram. Soc. 101 (1) (2018) 244–251.
[4] T. Ibn-Mohammed, C.A. Randall, K. Mustapha, J. Guo, J. Walker, S. Berbano, et al., Decarbonizing ceramic manufacturing: A techno-economic analysis of energy efficient sintering technologies in the functional materials sector, J. Eur. Ceram. Soc. 39 (16) (2019) 5213–5235.
[5] X. Wang, W. Lei, W. Lu, Novel ZnAl2O4-based microwave dielectric ceramics with machinable property and its application for GPS antenna, Ferroelectrics 388 (1) (2009) 80–87.
[6] D. Zhou, L.X. Pang, D.W. Wang, Z.M. Qi, I.M. Reaney, High quality factor, ultralow sintering temperature Li6B4O9 microwave dielectric ceramics with ultralow density for antenna substrates, ACS Sustain. Chem. Eng. 6 (2018) 11138–11143.
[7] R. Gheisari, H. Chamberlain, G. Chi-Tangyie, S. Zhang, A. Goulas, C.-K. Lee, A. Ghosh, et al., Multi-material additive manufacturing of low sintering temperature Bi2Mo2O9 ceramics with Ag floating electrodes by selective laser burnout, Virtual Phys. Prototyp. 15 (2) (2020) 133–147.
[8] H.H. Guo, D. Zhou, W.F. Liu, L.X. Pang, D.W. Wang, et al., Microwave dielectric properties of temperature-stable zircon-type (Bi,Ce)VO4 solid solution ceramics, J. American Ceramic Soc. 103 (1) (2020) 23–431.
[9] D. Zhou, L.X. Pang, D.W. Wang, C. Li, B.B. Jin, I.M. Reaney, High permittivity and low loss microwave dielectrics suitable for 5G resonators and low temperature co-fired ceramic architecture, J. Mater. Chem. C 5 (38) (2017) 10094–10098.
[10] D.J. Green, O. Guillon, J. Rçdel, Constrained sintering: a delicate balance of scales, J. Europ. Ceramic Soc. 28 (2008) 1451–1466.
[11] Z. Song, K. Song, B. Liu, P. Zheng, H.B. Bafrooei, W. Su, et al., Temperature dependent dielectric and Raman spectra and microwave dielectric properties of gehlenite-typed Ca2Al2SiO7, Int. J. Appl. Ceram. Technol. 17 (2) (2020) 771–777.
[12] Z. Tan, K. Song, H.B. Bafrooei, B. Liu, J. Wu, J. Xu, et al., The effects of TiO2 addition on microwave dielectric properties of Y3MgAl3SiO12 ceramic for 5G application, Ceram. Int. 46 (10) (2020) 15665–15669.
[13] Y. Ji, K. Song, X. Luo, B. Liu, H. Barzegar Bafrooei, D. Wang, Microwave dielectric properties of (1-x)Li2MoO4-xMg2SiO4 composite ceramics fabricated by cold sintering process, Front. Mater. 6 (2019) 256.
[14] Q. Lin, K. Song, B. Liu, H.B. Bafrooei, D. Zhou, W. Su, et al., Vibrational spectroscopy and microwave dielectric properties of AY2Si3O10 (A=Sr, Ba) ceramics for 5G applications, Ceram. Int. 46 (1) (2020) 1171–1177.
[15] S.S. Faouri, A. Mostaed, J.S. Dean, D. Wang, D.C. Sinclair, S. Zhang, et al., High quality factor cold sintered Li2MoO4–BaFe12O19 composites for microwave applications, Acta Mater. 166 (2019) 202–207.
[16] M. Väätäjä, H. Kähäri, K. Ohenoja, M. Sobocinski, J. Juuti, H. Jantunen, 3D printed dielectric ceramic without a sintering stage, Sci. Rep. 8 (2018) 15955.
[17] D. Wang, D. Zhou, S. Zhang, Y. Vardaxoglou, W.G. Whittow, D. Cadman, et al., Cold-sintered temperature stable Na0.5Bi0.5MoO4-Li2MoO4 microwave composite ceramics, ACS Sustain. Chem. Eng. 6 (2) (2018) 2438–2444.
[18] D. Zhou, L.X. Pang, D.W. Wang, I.M. Reaney, Novel water-assisting low firing MoO3 microwave dielectric ceramics, J. Eur. Ceram. Soc. 39 (7) (2019) 2374–2378.
[19] H. Kahari, M. Teirikangas, J. Juuti, H. Jantunen, Dielectric properties of Lithium molybdate ceramic fabricated at room temperature, J. Am. Ceram. Soc. 97 (11) (2014) 3378–3379.
[20] D. Wang, D. Zhou, K. Song, A. Feteira, C.A. Randall, I.M. Reaney, Cold sintered C0G multilayer ceramic capacitors, Adv. Electron. Mater. 5 (7) (2019), 1900025.

[21] S.C. Funahashi, J. Guo, H.Z. Guo, K. Wang, L.A. Baker, K. Shiratsuyu, et al., Demonstration of the cold sintering process study for the densification and grain growth of ZnO ceramics, J. Am. Ceram. Soc. 100 (3) (2017) 546–553.
[22] J.P. Ma, X.-M. Chen, W.-Q. Ouyang, J. Wang, H. Li, J.-L. Fang, Microstructure, dielectric, and energy storage properties of BaTiO3 ceramics prepared via cold sintering, Ceram. Int. 44 (1) (2018) 4436–4441.
[23] J.H. Seo, J. Guo, H. Guo, K. Verlinde, D.S.B. Heidary, R. Rajagopalan, et al., Cold sintering of a Li-ion cathode: LiFePO4-composite with high volumetric capacity, Ceramics Int. 43 (17) (2017) 15370–15374.
[24] W. Hong, L. Li, M. Cao, Plastic deformation and effects of water in room-temperature cold sintering of NaCl microwave dielectric ceramics, J. Am. Ceram. Soc. 101 (9) (2018) 4038–4043.
[25] D. Wang, S. Zhang, D. Zhou, K. Song, A. Feteira, Y. Vardaxoglou, et al., Temperature stable cold sintered (Bi0.95Li0.05)(V0.9Mo0.1)O4- Na2Mo2O7 microwave dielectric composites, Materials 12 (9) (2019) 1370.
[26] D. Wang, S. Zhang, G. Wang, Y. Vardaxoglou, W. Whittow, D. Cadman, et al., Cold sintered CaTiO3- K2MoO4 microwave dielectric ceramics for integrated microstrip patch antennas, Appl. Mater. Today 18 (2020), 100519.
[27] D. Wang, B. Siame, S. Zhang, G. Wang, X. Ju, J. Li, Z. Lu, et al., Direct integration of cold sintered, temperature-stable Bi2Mo2O9-K2MoO4 ceramics on printed circuit boards for satellite navigation antennas, J. Eur. Ceram. Soc. (2020), https://doi.org/10.1016/j.jeurceramsoc.2020.04.025.
[28] Y.B. Guo, J.-T. Ma, J.-X. Zhao, K. Du, Z.-T. Fang, Y.-Q. Zheng, et al., Low-temperature sintering and microwave dielectric properties of CaSnxSiO(3+2x)-based positive τf compensator, Ceram. Int. 44 (2018) 18209–18212.
[29] K. Du, X.-Q. Song, J. Li, J.-M. Wu, W.-Z. Lu, X.-C. Wang, W. Lei, Optimized phase compositions and improved microwave dielectric properties based on calcium tin silicates, J. Eur. Ceram. Soc. 39 (2019) 340–345.
[30] Y. Liu, P. Liu, C.X. Hu, Low-temperature preparation and microwave dielectric properties of cold sintered Li2Mg3TiO6 nanocrystalline ceramics, Ceramics Internationals 44 (17) (2018) 21047–21052.
[31] J. Guo, H. Guo, A.L. Baker, M.T. Lanagan, E.R. Kupp, G.L. Messing, C.A. Randall, A Cold sintering: A paradigm shift for processing and integration of ceramics, Angew. Chem. Int. Ed. 55 (1) (2016) 11457–11461.
[32] A. Baker, H.Z. Guo, J. Guo, C. Randall, Utilizing the cold sintering process for flexible-printable electroceramic device fabrication, J. Eur. Ceram. Soc. 99 (10) (2016) 3202–3204.
[33] A.M. Heyns, P.M. Harden, Evidence for the existence of Cr(IV) in chromium-doped malayaite Cr4+:CaSnOSiO4: a resonance Raman Study, J. Phys. Chem. Solids 60 (2) (1999) 277–284.
[34] S.Y. Vaselnia, M.K. Aminian, H. Motahari, R.D. Banadaki, A joint experimental and theoretical study on the structural, electronic and optical properties of malayaite and Chromium-doped malayaite structures as pigments, J. Phys. Chem. Solids 141 (2020), 109402.